FULL PAPER

BJC

British Journal of Cancer (2014) 111, 708–715 | doi: 10.1038/bjc.2014.324

Keywords: neuroblastoma; surgery; chemotherapy; controlled release; animal model

Surgery combined with controlled-release doxorubicin silk films as a treatment strategy in an orthotopic neuroblastoma mouse model

B Chiu*[,1], J Coburn[2], M Pilichowska[3], C Holcroft[4], F P Seib[5], A Charest[6] and D L Kaplan[2]

[1]Department of Surgery, University of Illinois at Chicago, 840 S. Wood Street, Suite 416, Chicago, IL 60612, USA; [2]Department of Biomedical Engineering, Tufts University, 4 Colby Street, Medford, MA 02155, USA; [3]Department of Pathology, Tufts Medical Center, 800 Washington Street, Box 115, Boston, MA 02111, USA; [4]Tufts Clinical and Translational Science Institute, Tufts Medical Center, 800 Washington Street, Boston, MA 02111, USA; [5]Strathclyde Institute of Pharmacy and Biomedical Sciences, University of Strathclyde, 161 Cathedral Street, Glasgow G4 0RE, UK and [6]Department of Neurosurgery, Tufts Medical Center, 800 Washington Street, Tufts Medical Center, Box 5609, Boston, MA 02111, USA

Background: Neuroblastoma tumour resection goal is maximal tumour removal. We hypothesise that combining surgery with sustained, local doxorubicin application can control tumour growth.

Methods: We injected human neuroblastoma cells into immunocompromised mouse adrenal gland. When KELLY cell-induced tumour volume was $>300\,mm^3$, 80–90% of tumour was resected and treated as follows: instantaneous-release silk film with 100 μg doxorubicin (100IR), controlled-release film with 200 μg (200CR) over residual tumour bed; and 100 and 200 μg intravenous doxorubicin (100IV and 200IV). Tumour volume was measured and histology analysed.

Results: Orthotopic tumours formed with KELLY, SK-N-AS, IMR-32, SH-SY5Y cells. Tumours reached $1800 \pm 180\,mm^3$ after 28 days, $2200 \pm 290\,mm^3$ after 35 days, $1280 \pm 260\,mm^3$ after 63 days, and $1700 \pm 360\,mm^3$ after 84 days, respectively. At 3 days post KELLY tumour resection, tumour volumes were similar across all groups ($P = 0.6210$). Tumour growth rate was similar in untreated *vs* control film, 100IV *vs* 100IR, and 100IV *vs* 200IV. There was significant difference in 100IR *vs* 200CR ($P = 0.0004$) and 200IV *vs* 200CR ($P = 0.0003$). Tumour growth with all doxorubicin groups was slower than that of control (P: <0.0001–0.0069). At the interface of the 200CR film and tumour, there was cellular necrosis, surrounded by apoptotic cells before reaching viable tumour cells.

Conclusions: Combining surgical resection and sustained local doxorubicin treatment is effective in tumour control. Administering doxorubicin in a local, controlled manner is superior to giving an equivalent intravenous dose in tumour control.

Neuroblastoma is the most common extracranial solid tumour in children (Brodeur, 2003; Maris *et al*, 2007), with a prevalence of 1 in 7000–10 000 live births. The tumour originates from the neural crest and presents in various locations along the sympathetic nervous system. It predominantly occurs in the abdomen, especially in the adrenal medulla (50%), but also develops in the chest (20%), neck (4%), or pelvis (2%). It is a highly aggressive tumour, where 10% of the patients with localised disease at diagnosis experience a relapse, and 20% of those tumours become refractory to treatment. With current therapy, the 5-year overall survival of patients diagnosed with metastatic disease remains poor (Matthay *et al*, 1999; Perez *et al*, 2000).

The challenges of treating patients with high-risk neuroblastoma are several. Between 20% and 30% of these tumours do not respond completely to induction therapy (Shafford *et al*, 1984). For those tumours that initially respond to chemotherapy, the tumour recurs in 20–30% of the cases (Park *et al*, 2008). The chemotherapy regimen includes agents such as doxorubicin, cyclophosphamide, and etoposide that can render the patient with side effects such as cardiomyopathy, haemorrhagic cystitis, and myelosuppression as

*Correspondence: Dr B Chiu; E-mail: bchiumd@uic.edu

Received 12 February 2014; revised 7 May 2014; accepted 13 May 2014; published online 12 June 2014

well as secondary malignancy such as breast or thyroid cancer (Rubino *et al*, 2003). Even after the toxic chemotherapeutic regimen, locally advanced tumours still cannot be completely resected because of adhesion to vital structures such as the renal vein or the superior mesenteric artery. Therefore, complete resection needs to be balanced by organ preservation (La Quaglia *et al*, 1994).

When surgeons are confronted with patients with 'seemingly unresectable' tumour burden, is there a strategy that can make resection or total gross resection possible? A series of surgical patients have demonstrated that the probability of local progression was 50% in unresected patients *vs* 10% in stage 4 patients undergoing gross total resection (La Quaglia *et al*, 2004). Furthermore, the overall survival rate in resected patients was 50% compared with 11% in unresected patients. Gross total resection offered a survival benefit for stage 4 patients. Therefore, it would be advantageous to develop strategies that augment the surgeons' ability to completely resect tumours with large burdens. Even increasing the percentage of tumour that can be safely removed without injuring or sacrificing vital structures may give more favourable clinical outcomes.

Local delivery of chemotherapeutic agents may enhance the results of tumour resection. Clinically, chemotherapeutic agents are administered locally to some malignancies including intravesical therapy for bladder cancer and hepatic arterial infusion therapy for hepatocellular carcinoma (van der Meijden *et al*, 1992; Tzoracoleftherakis *et al*, 1999). A very aggressive treatment option for cancers that have spread to the intraperitoneal lining uses perfusion to deliver heating chemotherapeutic agents throughout the intraperitoneal cavity (intraperitoneal hyperthermic chemoperfusion) after surgical removal of localised tumours (Ceelen *et al*, 2000). Implantable, carmustine-releasing polymer wafers (GLIADEL, Eisai Inc., Woodcliff Lake, NJ, USA) are used for high-grade malignant glioma and recurrent glioblastoma multiforme post resection (Brem *et al*, 1995; Westphal *et al*, 2006).

For many centuries, silk has been used as suture material because of its unique physical properties and excellent biocompatibility. More recently, silk-based surgical meshes (Allergan Inc., Irvine, CA, USA) have been approved for use in humans. Current efforts are geared towards using silk as a delivery vehicle of chemotherapy (Seib and Kaplan, 2012; Seib *et al*, 2013a, b) as well as other molecules, including adenosine, penicillin, and vaccines (Pritchard *et al*, 2010; Zhang *et al*, 2012; Pritchard *et al*, 2013). Silk is easily formulated into films, hydrogel, microparticles, nanoparticles, microneedles, or combination materials that are also 100% degradable *in vivo* (Rockwood *et al*, 2011; Tsioris *et al*, 2012; Seib and Kaplan, 2013; Seib *et al*, 2013a). This structural versatility, paired with the aqueous processing technology, provides an additional advantage when applying these silk-based drug delivery platforms in the biological environment. Furthermore, the drug release profile of the silk biopolymer can be varied from immediate release to slow release over months (Wang *et al*, 2007), allowing for tailored drug administration schedule to suit individual clinical scenarios.

We hypothesise that the margins of surgical resection can be safely extended by applying the chemotherapeutic agent to the residual tumour bed, thus decreasing the tumour growth rate after resection. In this report, we tested this hypothesis by first establishing an orthotopic xenograft mouse model of neuroblastoma followed by surgical resection after the tumour volume reached $>300\,mm^3$. We then applied doxorubicin locally by utilising silk films as a drug delivery platform. The films were engineered to achieve instantaneous release or an initial rapid release followed by a sustained drug release.

MATERIALS AND METHODS

Cell culture. Four neuroblastoma cell lines with different genetic makeup were used. Human neuroblastoma SK-N-AS cells (American Type Culture Collection (ATCC, Manassas, VA, USA)) were maintained in Dulbecco's modified Eagle's medium (DMEM, HyClone, Logan, UT, USA) supplemented with 10% fetal bovine serum, $100\,IU\,ml^{-1}$ penicillin, $100\,\mu g\,ml^{-1}$ streptomycin, and 0.1 mM non-essential amino acids. Human neuroblastoma IMR-32 cells (ATCC) were maintained in modified Eagle's medium (MEM, HyClone) supplemented with 10% fetal bovine serum, $100\,IU\,ml^{-1}$ penicillin, and $100\,\mu g\,ml^{-1}$ streptomycin. Human neuroblastoma SH-SY5Y cells (ATCC) were maintained in 1 : 1 mixture of MEM and F-12 media supplemented with 10% fetal bovine serum, $100\,IU\,ml^{-1}$ penicillin, and $100\,\mu g\,ml^{-1}$ streptomycin. Human neuroblastoma KELLY cells (Sigma-Aldrich, St Louis, MO, USA) were maintained in RPMI-1640 (HyClone) supplemented with 10% fetal bovine serum, $100\,IU\,ml^{-1}$ penicillin, $100\,\mu g\,ml^{-1}$ streptomycin, and 2 mM glutamine. All cells were maintained in a 5% CO_2 atmosphere at 37 °C and trypsin-passaged at 80% confluence.

Animal procedure. All mouse procedures were performed in accordance with Tufts University's recommendations for the care and use of animals and were maintained and handled under protocols approved by the Institutional Animal Care and Use Committee. All procedures were performed with female NCr nude mice or BALB/c mice (Taconic, Hudson, NY, USA) at 7 weeks of age. Procedures and ultrasound measurements were performed under general anaesthesia using isoflurane inhalation. At least five animals were used for each experimental group unless otherwise stated.

Creation of neuroblastoma tumours. A transverse incision was made on the left flank. The abdominal viscera were retracted medially and the retroperitoneal space was entered. The left adrenal gland was located, and 2 μl of phosphate-buffered saline (PBS) containing a predetermined cell number was injected into the adrenal gland via a 30G needle. The abdominal viscera were then returned into the abdominal cavity and the fascia and skin layers closed. Tumour formation was followed by ultrasound measurements, and the animals were killed when the tumour volume exceeded $1000\,mm^3$. The tumours and organs were removed and processed as detailed below. In addition, four animals that had received 10^6 KELLY cells were killed at postoperative day 3 ($n=2$) and day 14 ($n=2$).

Resection of neuroblastoma tumours and application of silk films. For the tumour resection model, tumours formed by injection of 10^6 KELLY cells were tracked by ultrasound. When the tumour reached $\sim 300\,mm^3$, surgical resection was performed. Briefly, a transverse incision was made on the left flank. The abdominal viscera were retracted medially and the retroperitoneal space entered. The left kidney was first located, and the tumour originating from the left adrenal gland identified. Using a combination of scalpel and electrocautery, ~80–90% of the tumour volume was excised. Electrocautery and direct pressure were used to maintain haemostasis of the residual tumour surface. In the experimental groups, a single, sterile, doxorubicin-containing silk film was placed on the tumour resection bed and the fascia and the skin were closed in separate layers. Instantly soluble or controlled-release silk films contained a nominal doxorubicin loading of 100 and 200 μg, respectively (denoted as 100IR and 200CR). The control groups consisted of surgical resection with no treatment (untreated), control insoluble silk film (control film), and tail vein injection of 100 μg doxorubicin (100IV) and 200 μg doxorubicin (200IV) in 100 μl of saline solution. Tumour volume was measured twice a week via ultrasound. Animals were killed when the tumour volume exceeded $1000\,mm^3$. The tumours and organs were processed as described below. Some animals that

received tumour resection and 200CR films were killed at 1 h ($n=2$), 24 h ($n=2$), and 72 h ($n=3$) after implantation.

High-frequency ultrasound. The mouse was secured to the stage in a prone position. Next, a VisualSonics Vevo 2100 Sonographic probe (Toronto, ON, Canada) was applied to the left flank to locate the left adrenal gland and the tumour. Serial cross-sectional images (0.076 mm between images) were taken. The tumour volume was measured using the 3-D reconstruction tool (Vevo Software v1.6.0).

Engineering of the silk films. Silk was isolated for *Bombyx mori* cocoons as previously described (Seib and Kaplan, 2012). Briefly, cocoons were boiled in 20 mM sodium carbonate for 30 min and then washed with deionised water. The resulting fibres were air dried and then dissolved in 9.3 M lithium bromide at 60 °C for 4 h. The solution was dialyzed (3.4 kDa MWCO, Piece, Rockford, IL, USA) against deionised water for 2 days. To produce 100IR films, 385 μl of 2% w/v silk fibroin solution containing 865 μg ml^{-1} doxorubicin-HCl (LC Laboratories, Woburn, MA, USA) was cast on an 11 mm × 17 mm polydimethylsiloxane mould. The solution was allowed to air dry overnight. The resulting films were cut to 7 mm × 11 mm, resulting in 100 μg doxorubicin-loaded, instantly soluble silk films. To produce 200CR films, 436 μl of 2% silk fibroin solution was cast on a 13 mm × 17 mm PDMS mould and air dried overnight. Then, 59 μl of 7 mg ml^{-1} doxorubicin was pipetted onto the silk film and air dried overnight. The resulting film was cut to 7 mm × 11 mm and the silk was physically crosslinked via water vapor annealing overnight at room temperature following a previously published method (Seib and Kaplan, 2012).

***In vitro* measurement of doxorubicin release from silk film.** Doxorubicin loading and release was determined by light absorbance at 482 nm using a SpectraMax M2 spectrophotometer (Molecular Devices, Sunnyvale, CA, USA). For quantification of soluble film loading, films were dissolved in PBS and absorbance values converted to concentration via a standard curve made in PBS. For quantification of insoluble film loading, films were dissolved using 100 μl 9.3 M lithium bromide at 60 °C for 30–60 min. The resulting solution was diluted with 900 μl PBS. Absorbance values were converted to concentration via a standard curve made in 0.93 M lithium bromide/PBS solution. *In vitro* release curves were generated via release in PBS. Briefly, samples were incubated in 1 ml of PBS under static conditions. At each time point, the entire volume of PBS was removed and replaced with fresh PBS to ensure sink conditions.

***In vivo* measurement of doxorubicin release from silk film.** After the female BALB/c mouse was anaesthetised with isoflurane inhalation, a transverse incision was made on the left flank. The abdominal viscera were retracted medially and the retroperitoneal space was entered. The left kidney and adrenal were identified and a 200CR film placed over them. The fascia and skin were closed in separate layers. Animals treated in this manner were randomly enrolled into one of the following groups, with each group consisted of five animals killed according to the prescribed time points: postoperative days 1, 2, 3, 7, 10, 14, 21, and 28. The films were retrieved after killing of animal. The remaining doxorubicin was quantified to generate the *in vivo* release profile as described above for loading of insoluble films. The 28- day implanted control films were used as background controls.

Morphologic examination. After the animals were killed, the tumours were removed, fixed in 10% buffered formalin, serially dehydrated and embedded in paraffin. Then, 5 μm thick sections were collected onto glass slides. Sections were stained with haematoxylin and eosin. To visualise proliferative cells, sections were stained using an anti-Ki67 antibody. To visualise apoptotic cells, sections were stained using the TUNEL assay (TACS-XL DAB *In Situ* Apoptosis Detection Kit, R&D Systems, Minneapolis, MN, USA). All sections were subjected to morphological examination by light microscopy.

Statistics. All animals that underwent resection and subsequent treatments were included in the statistical analysis at specific time points; all animals within a treatment group were excluded from subsequent tumour measures, as a group, when all animals within the group had reached the predetermined maximum tumour size range.

The analysis objective was to examine changes in tumour volume over time and compare tumour growth rates across experimental groups. As an initial step, ANOVA was used to compare the first measure of tumour volume (at postoperative day 3) across the six experimental groups. To estimate and compare tumour growth rates, we used a random effects model in which a different intercept and slope for each experimental group was estimated. This model does not require equal lengths of follow-up time to measure tumour growth rates. The model intercept for each treatment group represents the mean tumour volume at postoperative day 3, and the slope for each treatment group represents the change in tumour volume over time. The untreated group was used as the reference group in the model. Additional group comparisons were evaluated using prespecified two-group contrasts. Because of multiple testing, statistical significance was determined after controlling for the false discovery rate (Benjamini and Hochberg, 1995). Data for release studies and tumour volumes are presented as average ± s.d.

RESULTS

Tumour model establishment. Evaluation of the tumour model was performed using high-frequency ultrasound imaging. All tumour volumes were measured noninvasively with high-frequency ultrasound by taking serial cross-sections of the adrenal gland or tumour (Figure 1A). Three-dimensional reconstructions were then created from these cross-sections and measured manually to obtain the volumetric measurements (Figure 1B and C).

All four neuroblastoma cell lines were capable of establishing neuroblastoma tumour with a 10^6 cell injection into the adrenal gland of immunocompromised mice. The KELLY cells had the fastest rate of growth, reaching an average of 1800 ± 180 mm^3 after 28 days (Figure 2A). The SK-N-AS cells had a slightly slower growth rate, reaching 2200 ± 290 mm^3 after 35 days (Figure 2A). The IMR-32 cells required 63 days to reach 1280 ± 260 mm^3 (Figure 2A). SH-SY5Y had the slowest growth rate, reaching 1700 ± 360 mm^3 only after 84 days (Figure 2A).

Injection of 10^4 KELLY cells took longer (1940 ± 240 mm^3 after 56 days) (Figure 2B) to establish tumours compared with 10^6 KELLY cells (1800 ± 180 mm^3 after 28 days). Injection of 10^3 KELLY cells did not establish a tumour after 56 days (Figure 2B), and histological examination of these adrenal glands showed no tumour cell engraftment (data not shown). At 3 days after injecting 10^6 KELLY cells, there was extensive ischaemia within the adrenal gland and no detectable tumour engraftment (Figure 1D). The tumour was observed in the adrenal gland at 14 days (Figure 1E).

Controlled release of doxorubicin from silk films. Doxorubicin release from 200CR films was monitored *in vitro* and *in vivo*. During the *in vitro* release, ~100 μg of doxorubicin was released immediately. Over the following 30 days, ~40 μg of doxorubicin was released (Figure 3). The slow release portion of the release curve is comparable to previous literature (Seib and Kaplan, 2012). The 200CR films were designed to release 100 μg doxorubicin initially to elicit a rapid tumour response followed by a sustained release to facilitate slowing of tumour regrowth. *In vivo*, ~100 μg

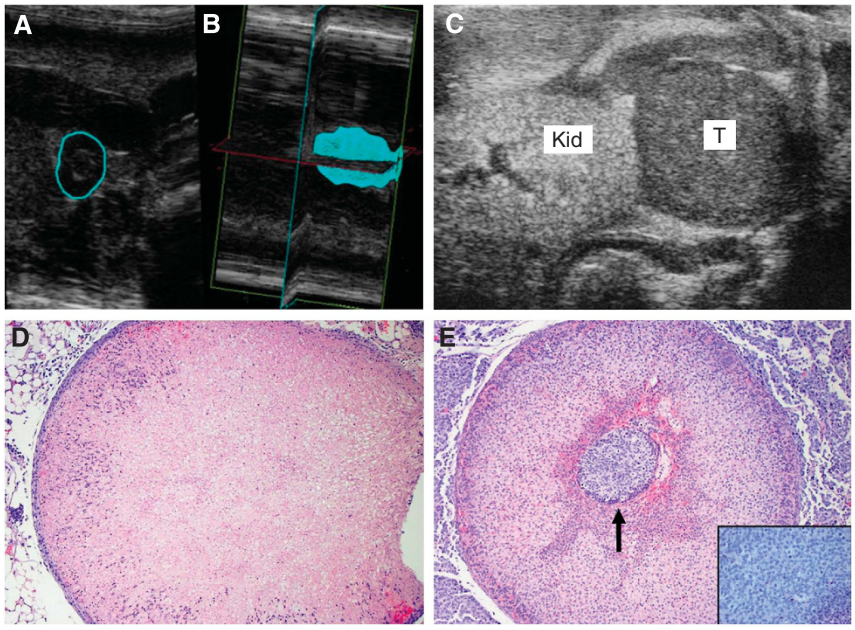

Figure 1. Ultrasound and histological imaging (haematoxylin and eosin stained) of 10^6 KELLY cell-induced tumour and the associated adrenal gland. (**A**) Ultrasound image of the cross-section of the adrenal gland. The hyperechoic centre denotes the medulla. (**B**) Three-dimensional reconstruction of the adrenal gland, from which the volume measurement was made. (**C**) A cross-sectional view of the tumour that was adjacent to the kidney. Kid = kidney; T = tumour. (**D**) The adrenal gland with extensive necrosis 3 days after 10^6 KELLY cells were injected (× 100). (**E**) The adrenal gland with intramedullary neuroblastoma 14 days after 10^6 KELLY cells were injected (× 100; arrow). The inset shows neuroblastoma cells at a higher power (× 1000, oil).

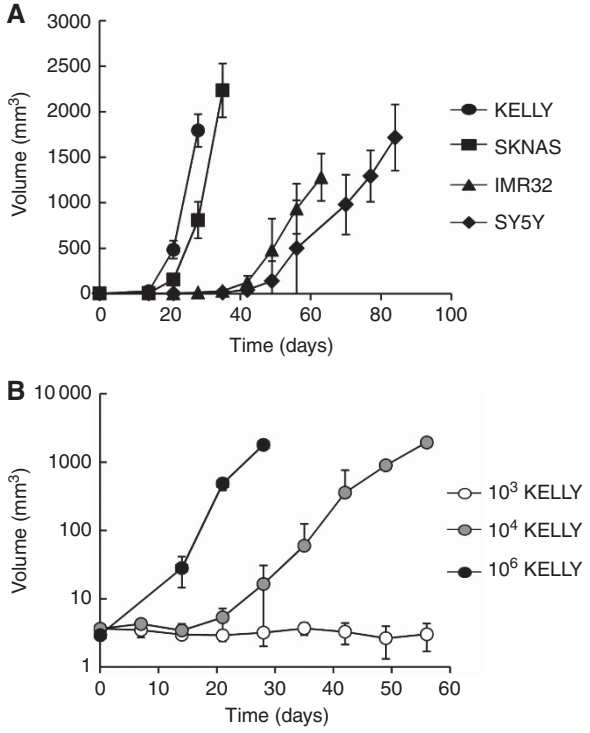

Figure 2. Tumour growth over time quantified by image analysis of ultrasound imaging. (**A**) Tumour volume at predetermined time points after injections with 10^6 KELLY, SK-N-AS, IMR-32, and SH-SY5Y cells. (**B**) Tumour volume at various time points after injections with 10^4 and 10^3 KELLY cells ($n = 5$).

of doxorubicin was also released immediately followed by slow release of 80 μg doxorubicin over the following 30 days (Figure 3). The major difference between the *in vitro* and *in vivo* release was

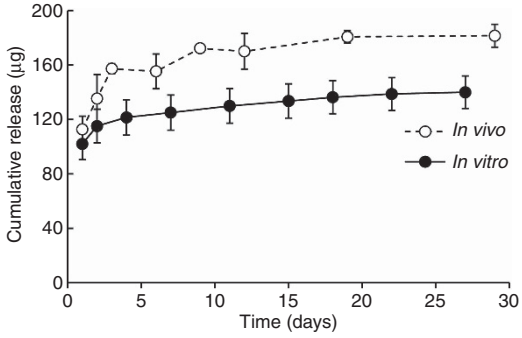

Figure 3. Cumulative doxorubicin released over time in the *in vitro* and *in vivo* setting. For *in vitro* release studies, doxorubicin is quantified in PBS. For the *in vivo* release studies, the remaining doxorubicin in the film is quantified and subtracted from the average initial loading (*in vitro* $n = 3$, *in vivo* $n = 3$–5).

observed within the first 4 days. Overlaying the release curves after the initial 4 days showed no significant differences in the release kinetics (data not shown).

Altered tumour growth kinetics upon implantation of doxorubicin-loaded silk films. For treatment studies, tumours were formed using 10^6 KELLY cells injected into the left adrenal gland. Once the tumour volume reached $>300\,mm^3$, the animal underwent an 80–90% tumour resection before it was enrolled in one of the following six experimental groups: (1) untreated, (2) control silk film, (3) 100IV, (4) 200IV, (5) 100IR, and (6) 200CR. Ultrasound measurements of the tumour volume began 3 days after tumour resection. At day 3, the mean tumour volume ranged from 22.3 to 42.1 mm^3 (Figure 4) with no significant differences among the six groups (ANOVA, $P = 0.6210$). Untreated tumours reached a volume of $1102.3 \pm 265.1\,mm^3$ after 17 days that was

comparable to control film-treated tumours of $1419.6 \pm 170.2\,mm^3$ ($P = 0.0764$ for growth rate comparison; Figure 5A). All doxorubicin-containing groups had significantly slower tumour growth (P value ranged from <0.0001 to 0.0069) compared with the control film group (Figures 5A–D). In animals that received 100IV or 200IV, the tumour volume reached $1018.3 \pm 408.2\,mm^3$ after 21 days and $1051.3 \pm 422.5\,mm^3$ after 28 days, respectively (growth rate comparison $P = 0.0465$, but not statistically significant after controlling for the false discovery rate; Figure 5A). In animals that received 100IR films, the tumour volume reached $1004.0 \pm 201.9\,mm^3$ after 28 days, significantly faster tumour growth compared with 200CR film-treated tumours ($928.7 \pm 389.6\,mm^3$ after 49 days, $P = 0.0004$; Figure 5B). The 100IR film treatment resulted in a similar tumour growth rate compared with 100IV treatment ($P = 0.0487$, not statistically significant after controlling for the false discovery rate; Figure 5C). However, treatment with 200CR films significantly decreased the tumour growth rate compared with 200IV injection ($P = 0.0003$; Figure 5D). The 200CR film treatment outperformed all of the other groups studied.

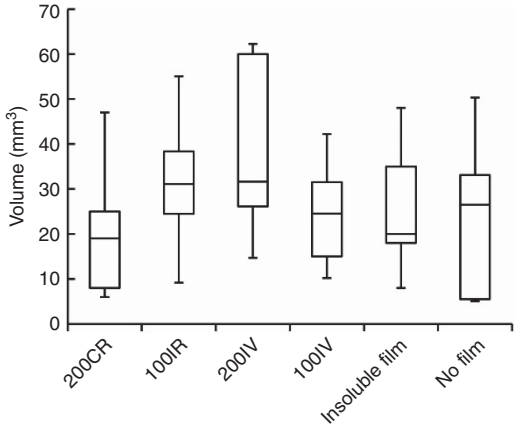

Figure 4. Box plot of the tumour volumes at postoperative day 3 (middle bars represent median values and, in this data set, the whiskers denote the minimum and maximum tumour volume, $n = 5$).

Histological assessment of tumours. Animals that received 200CR film treatment after resection of the original tumour were killed at day 49. Histological assessment of the tumours revealed that there was a zone of cellular necrosis immediately adjacent to the film (Figure 6A). This zone of cellular necrosis was surrounded by proliferative tumour cells evident by positively staining for Ki67 (Figure 6C). At the interface between the viable tumour cells and the zone of cellular necrosis, there appeared to be a transition zone of apoptotic cells (Figure 6B).

To further characterise the pathological changes associated with 200CR films, a short-term time course experiment was performed. Animals that underwent resection of the original adrenal tumour were either treated with control films, 200CR films, or left untreated. After the aforementioned treatments, the animals were killed at 1, 24, and 72 h. Untreated tumours or control film treated tumours showed predominantly viable tumour cells at 1 h (data not shown), 24 h (Figure 7A and B), and 72 h (Figure 7D and E). Tumours treated with 200CR film had necrotic cells adjacent to the film starting at 24 h (Figure 7C) that persisted through 72 h (Figure 7F).

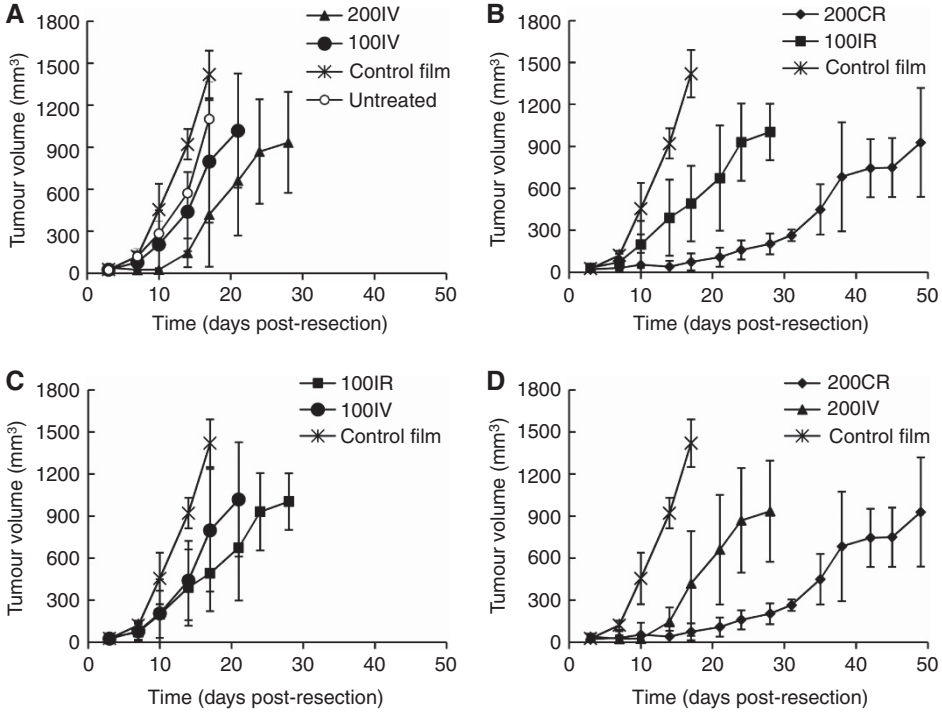

Figure 5. Postresection tumour volume *vs* time as measured by high-frequency ultrasound. (**A**) There were no differences between untreated and control film-treated tumour growth. Statistically different tumour growth was observed between both 100IV or 200IV when compared with control film-treated animals. (**B**) Tumour growth in both doxorubicin-loaded silk film treatments was statistically different than control film group. Tumours treated with 100IR grew faster than 200CR treated tumours. Animals treated with (**C**) 100 μg doxorubicin (IR or IV) and (**D**) 200 μg doxorubicin (CR or IV) had statistically different tumour growth than those treated with control film ($P<0.05$: 100IV *vs* control film; $P<0.005$: 200CR *vs* 100IR, 200CR *vs* 200IV; $P<0.0001$: 100IR *vs* control film, 200CR *vs* control film, 200IV *vs* control film).

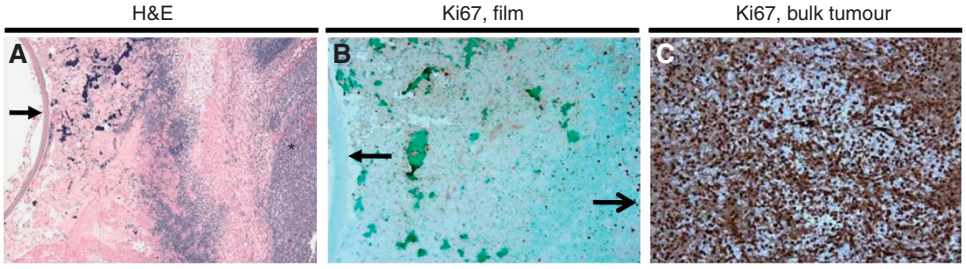

Figure 6. Histological analysis of 200CR film-treated tumour at day 49 post resection. (**A**) Haematoxylin and eosin staining of the tumour (× 40; *denotes viable tumour) At the silk film/tumour interface, a zone of cellular necrosis can be observed (small arrowhead denotes film). Ki67 staining of the tumour (**B**, × 200; **C**, × 200). At the interface between the viable tumour cells and the zone of cellular necrosis, there appeared to be a transition zone of apoptotic cells (**B**) (large arrowhead). Viable tumour cells surrounded the transition zone (**C**).

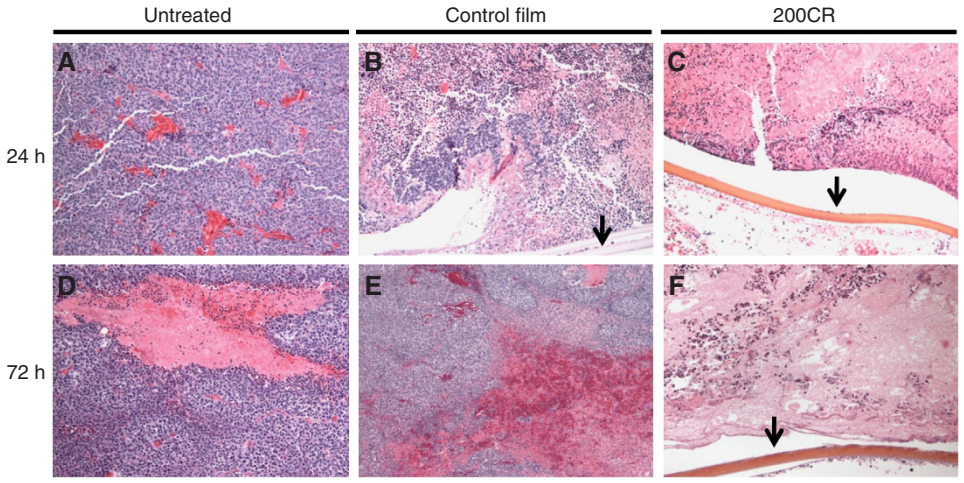

Figure 7. Haematoxylin and eosin staining of tumour bed at 1, 24 and 72 h post resection. Viable cells can be seen in the tumour bed at 24 and 72 h post resection that were untreated (**A** and **D**) and control film treated (**B** and **E**). However, 200CR film-treated tumour beds exhibited cellular necrosis at 24 h (**C**) and 72 h (**F**) post excision. Arrow denotes the silk film (**A–F**, × 100).

DISCUSSION

We have successfully demonstrated that four different neuroblastoma cell lines, KELLY, SK-N-AS, IMR-32, and SH-SY5Y, are capable of establishing adrenal tumours in an orthotopic xenograft injection mouse model. These four cell lines possess different genetic characteristics in terms of the MYCN amplification status and anaplastic lymphoma kinase (ALK) receptor status (Table 1). Morphological examination of the adrenal gland after the injection demonstrated initial extensive necrosis. The established adrenal tumour was composed of small cells, frequently in association with necrosis, and was showing brisk mitotic and apoptotic activity as seen in neuroblastoma.

No macroscopic or microscopic metastases were noted in our model as compared with the other published reports of orthotopic xenograft neuroblastoma animal models (Henriksson *et al*, 2004; Fuchs *et al*, 2009). One possible explanation is because of the use of NCr nude mice as opposed to SCID mice that are more permissive to metastasis (Mueller and Reisfeld, 1991). Another potential reason relates to the technique used for tumour injection. In the orthotopic injection neuroblastoma model reported by Henriksson *et al* (2004), a 10 μl injection volume was used. As the mouse adrenal gland is only $\sim 3\,mm^3$, most of the tumour cells injected spill into the abdominal cavity as described by the authors, inoculating other tissues in the vicinity. In our model, we have concentrated the tumour cells requiring only a 2 μl injection volume. Furthermore, a needle with a shortened bevel was used so that the entire needle opening was within the adrenal gland during injection.

Table 1. Genetic characterisations of the neuroblastoma cell lines

Cell line	KELLY	IMR-32	SH-SY5Y	SK-N-AS
MYCN status	Amplified	Amplified	Nonamplified	Nonamplified
ALK mutation	Yes	No	Yes	No

Abbreviation: ALK = anaplastic lymphoma kinase.

In our model, we used high-frequency ultrasound to perform repeat, longitudinal, and noninvasive determinations of the tumour volume. Using this fast and accurate methodology to monitor tumour growth parameters, Teitz *et al* (2011) compared the use of ultrasound with that of bioluminescence and magnetic resonance imaging (MRI) for assessing tumour volume in an orthotopic xenograft neuroblastoma model. They found excellent volume measurement correlation between the different modalities. The MRI provided superior detail in tumour origin and composition but at a higher cost and much longer imaging time. The combination of a reliable, reproducible, and efficient orthotopic injection model with an accurate, noninvasive volume measurement system creates an ideal platform for preclinical testing of therapeutic agents.

In our work, there was a minimum cell number required to establish an orthotopic neuroblastoma xenograft. With a

decreasing number of cells injected, the time required to establish the tumour is increased. No tumour was observed with 10^3 KELLY cells injected. Histological examinations of these adrenal glands did not demonstrate tumour formation. These finding with the KELLY cell line suggest that certain percentage of these cells possess a tumour-initiating property, and a threshold of cell number needs to be achieved to ensure these cells are present. The presence of tumour-initiating cells have been demonstrated in human tumour samples obtained from pre- and post-treatment neuroblastoma tumours from the bone marrow of patients who had relapsed after multiple courses of chemotherapy and from the bone marrow of patients in remission (Hansford *et al*, 2007).

Frequently, surgery is an integral component of clinical cancer care. The ability to closely model the behaviour of tumours in their orthotopic location after undergoing surgical resection, mimicking the clinical scenario, can be key to improving the effectiveness of surgical therapy. Our model meets this need by establishing a sizable neuroblastoma tumour in the adrenal gland as well as allowing for surgical resection of 80–90% of the tumour, similar to the frequently encountered clinical scenarios. Davis *et al* (1990) combined neuroblastoma tumour resection with intraoperative photodynamic therapy to demonstrate the reduction in the rate of tumour recurrence. However, this report could not accurately quantify the amount of tumour before or after resection. Pastorino *et al* (2008) utilised surgical resection in their orthotopic neuroblastoma mouse model and quantified the perioperative tumour size with a luciferase/bioluminescence system. Despite being a frequently used research tool, the bioluminescence system is not a clinical option. The ultrasound system we used for tumour volume measurement is more readily translated clinically.

The animals were able to tolerate the stress of the surgical tumour resection. The haemostatic manoeuvres such as direct pressure and electrocautery were sufficient to ensure a safe procedure. We also found that breaking the tumour capsule and spilling tumour cells into the abdominal cavity did not result in dissemination of tumour within the abdominal cavity. In fact, the residual tumour remained at the original tumour bed serving as the focus of additional tumour growth. In addition, we did not observe any tissue ischaemia or organ loss in our series.

We found that the tumour growth rate was not significantly different between untreated and control film-treated residual tumour beds. Therefore, the presence of silk films alone does not alter tumour regrowth. There was a substantial difference between animals that received an intravenous bolus of either 100 or 200 μg of doxorubicin compared with those with control films, with the better tumour response for the latter treatment group. Variable blood supply to the residual tumour bed could have led to a variable amount of doxorubicin delivered, thus resulting in different degrees of drug exposure between the animals receiving different intravenous doses (el-Kareh and Secomb, 1997).

Treating the residual tumour with one application of 100 μg doxorubicin via intravenous injection or instantaneous released film placement resulted in similar tumour growth rate. However, applying doxorubicin locally *vs* systemically could lead to fewer systemic side effects such as cardiomyopathy. Local application of chemotherapeutic agents may be a less toxic strategy for the overall tumour treatment protocol and warrants further investigation.

Alternatively, when the dosage of the doxorubicin was doubled in the locally delivered silk films, the tumour growth rate was slowed significantly. The effect of doxorubicin on slowing tumour growth appeared to be more effective when the 200CR film was utilised compared with 200IV injections. The controlled-release nature of the silk platform clearly demonstrated the advantage of applying small doses of doxorubicin over time as opposed to one bolus dose. Our local delivery system allows for complete availability of the drug to the tumour, whereas in IV-administered drug, pharmacokinetic/pharmacodynamics dictate the bioavailability to the tumour. Coupling the local delivery with sustained release resulted in superior slowing of tumour growth because of the constant administration of drug directly to the tumour. There are many other factors that may have played a role in the effects seen with the local, sustained-release films. The controlled release of doxorubicin may create an environment that continually eliminated cancer stem cells (Reya *et al*, 2001) or maintained the total tumour cells just below a critical number to spur exponential tumour growth, as observed when too few cells were injected for tumour formation. Furthermore, the tumour microenvironment may have been altered by doxorubicin (Kang *et al*, 2013).

Doxorubicin has been shown to induce apoptosis through the CD95 system (Fulda *et al*, 1997). Histological examination of the tumours revealed that tumour cell death was the result of local effect rather than effects of systemic doxorubicin absorption. This is evident by cell death radiating away from the 200CR film through parts of the tumour. Our histological observation suggested that doxorubicin contained within the controlled-release silk film was diffused across the tumour, resulting in apoptosis and subsequent necrosis.

Extending the findings of our work to the clinical setting, there are some issues to be considered. First, the tumour-bearing animals are cytotoxic naive before resection and application of the doxorubicin-loaded silk films. Clinically, patients with advanced-stage neuroblastoma would have previously been exposed to cytotoxic therapy before surgery (Maris, 2010). Previous exposure to doxorubicin could result in the tumour harbouring doxorubicin-resistant cells (Maris, 2010), rendering the doxorubicin-loaded silk film less effective. As a higher effective doxorubicin dose can be delivered locally compared with that delivered systemically, we speculate that the small amount of tumour remaining after resection, possibly containing doxorubicin-resistant cells, can be overcome by sustained local application of doxorubicin. Second, despite the large size of the tumour described in our model, it is localised to the adrenal gland. However, locally advanced neuroblastoma tumours in patients frequently involve multiple sites (Maris, 2010). A potential solution will be to apply individual drug-loaded films at multiple sites. This approach will be ineffective if the tumour is already systemically disseminated.

In conclusion, we have shown that combining surgical resection with a doxorubicin-loaded, sustained-release silk film system is an effective strategy in decreasing neuroblastoma tumour growth. Future studies in characterising the local/systemic distribution of the drug as well as potential systemic toxicity will be essential in considering this strategy in a clinical setting.

ACKNOWLEDGEMENTS

The project described was supported by the National Center for Advancing Translational Sciences, National Institutes of Health, Grant Numbers UL1 TR000073, UL1 TR001064, and P41 EB002520.

REFERENCES

Benjamini Y, Hochberg Y (1995) Controlling the false discovery rate: a practical and powerful approach to multiple testing. *J R Stat Soc Ser B Stat Methodol* **57**: 289–300.

Brem H, Piantadosi S, Burger PC, Walker M, Selker R, Vick NA, Black K, Sisti M, Brem S, Mohr G, Muller P, Morawetz R, Schold SC (1995) Placebo-controlled trial of safety and efficacy of intraoperative controlled delivery by biodegradable polymers of chemotherapy for recurrent gliomas. *Lancet* **345**: 1008–1012.

Brodeur GM (2003) Neuroblastoma: biological insights into a clinical enigma. *Nat Rev Cancer* **3**: 203–216.

Ceelen WP, Hesse U, de Hemptinne B, Pattyn P (2000) Hyperthermic intraperitoneal chemoperfusion in the treatment of locally advanced intra-abdominal cancer. *Br J Surg* **87**: 1006–1015.

Davis RK, Smith LF, Thurgood RF, Kereszti Z, Straight RC (1990) Intraoperative phototherapy (PDT) and surgical resection in a mouse neuroblastoma model. *Lasers Surg Med* **10**: 275–279.

el-Kareh AW, Secomb TW (1997) Theoretical models for drug delivery to solid tumors. *Crit Rev Biomed Eng* **25**: 503–571.

Fuchs D, Christofferson R, Stridsberg M, Lindhagen E, Azarbayjani F (2009) Regression of orthotopic neuroblastoma in mice by targeting the endothelial and tumor cell compartments. *J Transl Med* **7**: 16.

Fulda S, Sieverts H, Friesen C, Herr I, Debatin KM (1997) The CD95 (APO-1/Fas) system mediates drug-induced apoptosis in neuroblastoma cells. *Cancer Res* **57**: 3823–3829.

Hansford LM, McKee AE, Zhang L, George RE, Gerstle JT, Thorner PS, Smith KM, Look AT, Yeger H, Miller FD, Irwin MS, Thiele CJ, Kaplan DR (2007) Neuroblastoma cells isolated from bone marrow metastases contain a naturally enriched tumor-initiating cell. *Cancer Res* **67**: 11234–11243.

Henriksson KC, Almgren MA, Thurlow R, Varki NM, Chang CL (2004) A fluorescent orthotopic mouse model for reliable measurement and genetic modulation of human neuroblastoma metastasis. *Clin Exp Metastasis* **21**: 563–570.

Kang TH, Mao CP, Lee SY, Chen A, Lee JH, Kim TW, Alvarez RD, Roden RB, Pardoll D, Hung CF, Wu TC (2013) Chemotherapy acts as an adjuvant to convert the tumor microenvironment into a highly permissive state for vaccination-induced antitumor immunity. *Cancer Res* **73**: 2493–2504.

La Quaglia MP, Kushner BH, Heller G, Bonilla MA, Lindsley KL, Cheung NK (1994) Stage 4 neuroblastoma diagnosed at more than 1 year of age: gross total resection and clinical outcome. *J Pediatr Surg* **29**: 1162–1165. discussion 1165-1166.

La Quaglia MP, Kushner BH, Su W, Heller G, Kramer K, Abramson S, Rosen N, Wolden S, Cheung NK (2004) The impact of gross total resection on local control and survival in high-risk neuroblastoma. *J Pediatr Surg* **39**: 412–417.

Maris JM (2010) Recent advances in neuroblastoma. *N Engl J Med* **362**: 2202–2211.

Maris JM, Hogarty MD, Bagatell R, Cohn SL (2007) Neuroblastoma. *Lancet* **369**: 2106–2120.

Matthay KK, Villablanca JG, Seeger RC, Stram DO, Harris RE, Ramsay NK, Swift P, Shimada H, Black CT, Brodeur GM, Gerbing RB, Reynolds CP (1999) Treatment of high-risk neuroblastoma with intensive chemotherapy, radiotherapy, autologous bone marrow transplantation, and 13-cis-retinoic acid. Children's Cancer Group. *N Engl J Med* **341**: 1165–1173.

Mueller BM, Reisfeld RA (1991) Potential of the scid mouse as a host for human tumors. *Cancer Metastasis Rev* **10**: 193–200.

Park JR, Eggert A, Caron H (2008) Neuroblastoma: biology, prognosis, and treatment. *Pediatr Clin North Am* **55**: 97–120.

Pastorino F, Di Paolo D, Piccardi F, Nico B, Ribatti D, Daga A, Baio G, Neumaier CE, Brignole C, Loi M, Marimpietri D, Pagnan G, Cilli M, Lepekhin EA, Garde SV, Longhi R, Corti A, Allen TM, Wu JJ, Ponzoni M (2008) Enhanced antitumor efficacy of clinical-grade vasculature-targeted liposomal doxorubicin. *Clin Cancer Res* **14**: 7320–7329.

Perez CA, Matthay KK, Atkinson JB, Seeger RC, Shimada H, Haase GM, Stram DO, Gerbing RB, Lukens JN (2000) Biologic variables in the outcome of stages I and II neuroblastoma treated with surgery as primary therapy: a Children's Cancer Group study. *J Clin Oncol* **18**: 18–26.

Pritchard E, Szybala C, Boison D, Kaplan DL (2010) Silk fibroin encapsulated powder reservoirs for sustained release of adenosine. *J Control Release* **144**: 159–167.

Pritchard EM, Valentin T, Panilaitis B, Omenetto F, Kaplan DL (2013) Antibiotic-releasing silk biomaterials for infection prevention and treatment. *Adv Funct Mater* **23**: 854–861.

Reya T, Morrison SJ, Clarke MF, Weissman IL (2001) Stem cells, cancer, and cancer stem cells. *Nature* **414**: 105–111.

Rockwood DN, Preda RC, Yucel T, Wang X, Lovett ML, Kaplan DL (2011) Materials fabrication from Bombyx mori silk fibroin. *Nat Protoc* **6**: 1612–1631.

Rubino C, Adjadj E, Guerin S, Guibout C, Shamsaldin A, Dondon MG, Valteau-Couanet D, Hartmann O, Hawkins M, de Vathaire F (2003) Long-term risk of second malignant neoplasms after neuroblastoma in childhood: role of treatment. *Int J Cancer* **107**: 791–796.

Seib FP, Jones GT, Rnjak-Kovacina J, Lin Y, Kaplan DL (2013a) pH-Dependent anticancer drug release from silk nanoparticles. *Adv Healthc Mater* **2**: 1606–1611.

Seib FP, Kaplan DL (2012) Doxorubicin-loaded silk films: drug-silk interactions and in vivo performance in human orthotopic breast cancer. *Biomaterials* **33**: 8442–8450.

Seib FP, Kaplan DL (2013) Silk for drug delivery applications: opportunities and challenges. *Israel J Chem* **53**: 756–766.

Seib FP, Pritchard EM, Kaplan DL (2013b) Self-assembling doxorubicin silk hydrogels for the focal treatment of primary breast cancer. *Adv Funct Mater* **23**: 58–65.

Shafford EA, Rogers DW, Pritchard J (1984) Advanced neuroblastoma: improved response rate using a multiagent regimen (OPEC) including sequential cisplatin and VM-26. *J Clin Oncol* **2**: 742–747.

Teitz T, Stanke JJ, Federico S, Bradley CL, Brennan R, Zhang J, Johnson MD, Sedlacik J, Inoue M, Zhang ZM, Frase S, Rehg JE, Hillenbrand CM, Finkelstein D, Calabrese C, Dyer MA, Lahti JM (2011) Preclinical models for neuroblastoma: establishing a baseline for treatment. *PLoS One* **6**: e19133.

Tsioris K, Raja WK, Pritchard EM, Panilaitis B, Kaplan DL, Omenetto FG (2012) Fabrication of silk microneedles for controlled-release drug delivery. *Adv Funct Mater* **22**: 330–335.

Tzoracoleftherakis EE, Spiliotis JD, Kyriakopoulou T, Kakkos SK (1999) Intra-arterial versus systemic chemotherapy for non-operable hepatocellular carcinoma. *Hepatogastroenterol* **46**: 1122–1125.

van der Meijden AP, Kurth KH, Oosterlinck W, Debruyne FM (1992) Intravesical therapy with adriamycin and 4-epirubicin for superficial bladder cancer: the experience of the EORTC GU Group. *Cancer Chemother Pharmacol* **30**(Suppl): S95–S98.

Wang X, Wenk E, Matsumoto A, Meinel L, Li C, Kaplan DL (2007) Silk microspheres for encapsulation and controlled release. *J Control Release* **117**: 360–370.

Westphal M, Ram Z, Riddle V, Hilt D, Bortey E. Executive Committee of the Gliadel Study Group (2006) Gliadel wafer in initial surgery for malignant glioma: long-term follow-up of a multicenter controlled trial. *Acta Neurochir (Wien)* **148**: 269–275discussion 275.

Zhang J, Pritchard E, Hu X, Valentin T, Panilaitis B, Omenetto FG, Kaplan DL (2012) Stabilization of vaccines and antibiotics in silk and eliminating the cold chain. *Proc Natl Acad Sci USA* **109**: 11981–11986.